

Low-Temperature Reactions | Hot Paper |

Ho-Mediated Alkyne Reactions at Low Temperatures on Ag(111)

Raphael Hellwig,^{*,[a]} Martin Uphoff,^[a] Tobias Paintner,^[a] Jonas Björk,^[b] Mario Ruben,^[c, d] Florian Klappenberger,^{*,[a]} and Johannes V. Barth^[a]

Abstract: Low-temperature approaches to catalytic conversions promise efficiency, selectivity, and sustainable processes. Control over certain coupling reactions can be obtained via the pre-positioning of reactive moieties by self-assembly. However, in the striving field of on-surface synthesis atomistic precision and control remains largely elusive, because the employed coupling reactions proceed at temperatures beyond the thermal stability of the supramolecular templates. Here, utilizing scanning tunneling microscopy, we demonstrate terminal alkyne on-surface reactions mediated by Ho atoms at a weakly reactive Ag(111) substrate at low-temperatures. Density functional theory calculations confirm the catalytic activity of the involved adatoms. Pre-deposited

Ho induces alkyne dehydrogenation starting at substrate temperatures as low as 100 K. Ho arriving at molecularly pre-covered surfaces held at 130 and 200 K produces covalent enyne-linked dimers and initiates cyclotrimerization, respectively. Statistical product analysis indicates a two-step pathway for the latter, whereby the enyne intermediates influence the distribution of the products. High chemoselectivity results from the absence of cyclotetramerization and diyne-forming homocoupling. Our analysis indicates that mainly the arriving Ho adatoms enable the coupling. These findings support the concept of dynamic heterogeneity by single-atom catalysts and pave the way for alternative means to control on-surface reactions.

Introduction

Low-temperature approaches to covalent reactions have impacted various fields of chemistry such as gold catalysis,^[1,2] Schiff base complexes^[3] and nanoparticles.^[4] With the milder conditions required, they not only allow higher efficiency,^[5] but also promise an access to sustainable chemistry.^[2] When targeting the cross-coupling of organic compounds, by reducing the necessary thermal activation, compatibility with often sensitive functional groups can be achieved.^[6] Prepositioning of reactive moieties by molecular self-assembly controlled via such functional groups is frequently used for reaction selectivity. For ex-

ample, this method was key to steer the formation of two-dimensional polymers.^[7,8] Recently, it was demonstrated that hydrogen-bonding motifs facilitate quantum mechanical tunneling leading to enhanced product formation at reduced temperature.^[9]

On-surface synthesis of covalent scaffolds and carbon-based materials under ultra-high vacuum (UHV) conditions is currently emerging as a most promising approach toward atom-precise functional architectures.^[10–16] Coupling of rationally designed precursors on metal substrates has been achieved via a variety of reactions including Ullmann-type aryl–aryl coupling,^[17,18] condensation reactions,^[19–23] transition metal-assisted polymerization^[24] and cyclotrimerization of acetyls.^[25] As a new route to synthesize hydrocarbon-based scaffolds, the coupling of alkyne-functionalized monomers on metal surfaces has gained increasing importance over recent years.^[26–29] The resulting polymeric materials are highly attractive owing to tunable electronic properties^[30–32] and potential technological applications^[17,19, 33, 34] as molecular sieves, energy storage units,^[35] molecular nanocircuits and host–guest interactions.

For exploiting the full potential of the on-surface approach, it would be highly desirable to control reactions via the above-mentioned self-assembly controlled prepositioning of precursors. So far, however, the annealing-induced coupling reactions proceed at temperatures above the thermal stability of the supramolecular structures formed from the involved organic compounds.

Here, we introduce a low-temperature on-surface carbon-coupling approach enabling the linkage of precursors much below room temperature (RT). More precisely, we employ Ho

[a] Dr. R. Hellwig, M. Uphoff, T. Paintner, Dr. F. Klappenberger, Prof. Dr. J. V. Barth
Physics Department E20, Technical University of Munich
85748 Garching (Germany)
E-mail: raphael.hellwig@tum.de
florian.klappenberger@tum.de

[b] Dr. J. Björk
Department of Physics, Chemistry and Biology (IFM)
Linköping University, 58183 Linköping (Sweden)

[c] Prof. Dr. M. Ruben
Institute für Nanotechnologie
Karlsruher Institut für Technologie (KIT)
76344 Eggenstein-Leopoldshafen (Germany)

[d] Prof. Dr. M. Ruben
Institut de Physique et Chimie de Matériaux de Strasbourg (IPCMS)
CNRS-Université de Strasbourg
67034 Strasbourg (France)

Supporting information and the ORCID identification number(s) for the author(s) of this article can be found under:
<https://doi.org/10.1002/chem.201803102>

adatoms as catalytic centers on a weakly reactive Ag(111) substrate for establishing covalent linkages between 1,3,5-tris(4-ethynylphenyl)benzene (Ext-TEB) monomers. Our Ho evaporation process is based on thermal sublimation by passing a current through a Ho foil. While transition elements like Pd are in widespread use in today's alkyne-based organochemistry,^[36] little attention has been paid to the catalytic properties of lanthanide centers. The latter have become of high interest for interfacial metal-organic coordination structures,^[37,38] near-infrared luminescence^[39] and single-atom magnetism.^[40] Recently, it was shown that lanthanum atoms catalyze carbon-carbon bond formation toward 3D graphene, when trapped together with acetylene molecules within the pores of zeolite template structures.^[41]

Here, the combination of terminal alkyne groups with the catalytic lanthanide centers renders possible two low-temperature reaction pathways, which are presented in Figure 1. Intri-

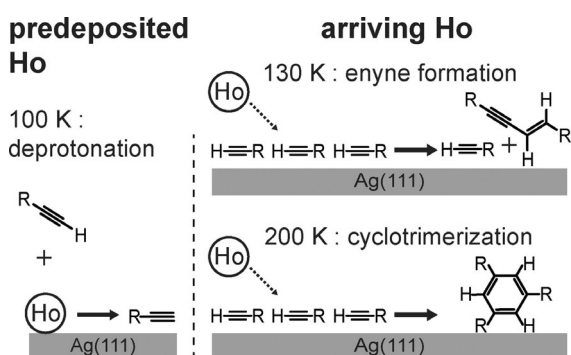


Figure 1. Ho-initiated reaction paths with terminal alkynes. (left) Predeposited thermalized Ho atoms induce alkyne deprotonation. (right) Arriving Ho atoms trigger C–C coupling reactions: enyne formation at 130 K and cyclotrimerization at 200 K.

guingly, for preparations, where Ho is dosed before Ext-TEB deposition, the Ho adsorbates on Ag(111) mainly induce alkyne dehydrogenation (Figure 1, left). The second reaction route is triggered by arriving Ho atoms (Figure 1, right) and enables precursor coupling at substrate temperatures as low as 130 K, in stark contrast to previous reports on heteroatom-catalyzed coupling^[42,43] with much higher activation barriers requiring substrate temperatures well above room temperature (ca. 400 K).

At such remarkably mild reaction conditions we observe the selective formation of enyne motifs within dimeric and oligomeric structures. For Ho dosage at 200 K, isolated trimers as well as hydrocarbon nanomeshes are created through cyclotrimerization. Noteworthy, homocoupling of terminal alkynes^[26] is entirely absent under the employed reaction conditions. Our analysis of the mechanism reveals that predominantly arriving Ho adatoms bestow a hitherto unrecognized dynamic heterogeneity to the interface triggering the coupling at low temperature. The unexpected catalytic activity is advantageous over other coupling scenarios requiring far higher substrate temperatures, which may entail spurious side reactions, release of adversely affecting dissociation products (e.g. halogens), and mo-

nomer desorption. Importantly, reactions at such temperature open novel avenues toward controlling on-surface coupling reactions via prepositioned precursors. Moreover, our findings lend support to the concept of single-atom catalysis mediated by metal adatoms.^[44, 45]

Results and Discussion

Molecular self-assembly and Ho-catalyzed deprotonation of terminal alkynes

Prior to investigating the potentially complex interaction of Ho adatoms with the organic compound, it is necessary to characterize the individual components. First, a sub-monolayer (sub-ML) amount of Ext-TEB (1 ML of Ext-TEB corresponds to a saturated layer of molecules covering the entire sample in a periodic densely-packed structure) was deposited on the clean Ag(111) sample at a substrate temperature of 130 K. The sample was cooled down to liquid He temperatures and characterized by STM. As depicted in Figure 2a, the molecules condensed into a densely packed adlayer stabilized by weak non-covalent interactions, which confirms the high mobility of Ext-TEB on Ag(111) at such temperatures observed earlier.^[46] The

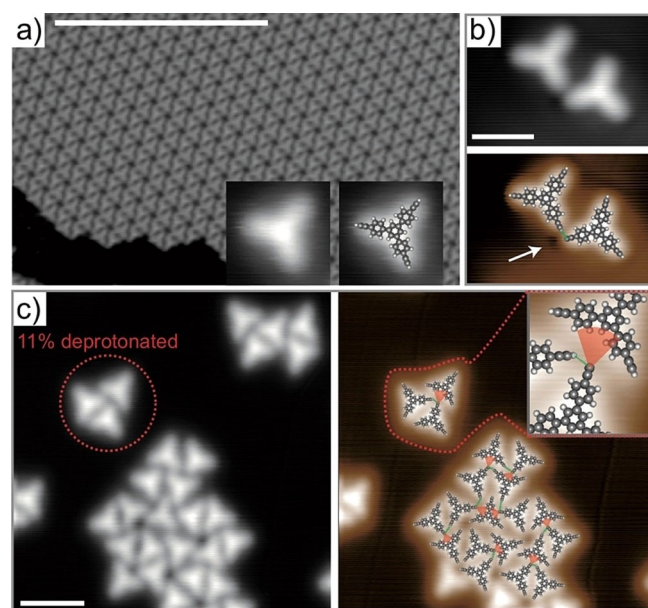


Figure 2. Ho-initiated deprotonation of Ext-TEB. STM topographs with superimposed molecular model and color-coded contrast (adjoined images).

(a) STM topographs of pristine monomer phase and single monomer with superimposed model (inset). After Ho dosage, pristine structure dissolved (b,c). (b) Twofold ionic hydrogen bonding motif: deprotonated alkyne interacts with intact alkyne moiety (green line). White arrow indicates depression attributed to alkynyl unit. (c) Threefold ionic hydrogen bonding motif (within red contour and magnified in inset): deprotonated alkyne faces an intact alkyne (green line) and a phenyl moiety (red-colored circle segment). An extended aggregate is built up from threefold motifs (green lines and red-colored circle segments). Preparation details for (b): Ho dosage (0.004 ML Ho) at 200 K, then molecular deposition (3 min) at 200 K; no sample annealing. Preparation details for (c): Ho dosage (0.01 ML Ho) at 93 K, then molecular deposition (3 min) at 92 K followed by sample annealing at 108 K for 10 min; then post-annealing at 200 K for 10 min. Tunneling parameters V_t, I_t : (a) 1 V, 0.3 nA (inset: 0.5 V, 0.3 nA); (b) 1 V, 0.1 nA; (c–e) –0.01 V, 0.1 nA. Scale bars: (a) 20 nm; (b) 3 nm; (c–e) 1.6 nm.

intact monomers are imaged as nearly triangular-shaped protrusions, the inset shows an isolated Ext-TEB monomer with and without a superimposed molecular model. Noteworthy, the STM data shows that the amount of impurities under such preparation conditions is negligibly low, and confirms the absence of potential organosilver structures^[47,48] and homocoupling products^[26,27,48] at such a low deposition temperature.

Next, we characterized the clean Ag(111) sample decorated by a sub-ML of Ho at 93 K, for which 1 ML is defined as one Ho atom for each topmost Ag atom. After Ho dosage, the sample was immediately transferred to the STM. We encountered large Ho clusters (see Supporting Information Figure S1a) evincing significant mobility and island growth of adsorbed Ho at low temperatures. High adsorbate mobility is well known for 4f metal elements, for example, Ce dosed *in situ* at 3.9 K on Ag(111) forms a well-ordered Ce superlattice at that temperature, whereby Ce dimerization sets in already at 4.8 K.^[49]

To investigate the behavior of Ho adsorbates toward terminal alkyne reactions, we started off by preparing a sample at the lowest temperature possible within our setup. We first dosed Ho (ca. 0.01 ML in 30 s) and then deposited Ext-TEB (ca. 0.20 ML in 3 min (minutes)) both at $T_{\text{sample}} = 92$ K and kept the sample stable at 108 K for 10 min before transferring it to the microscope. According to Supporting Information Figure S1b, we observed irregular patches of molecules with incorporated dot-like protrusions. The uniformity of the protrusions in close-up images (Figure S1c) indicates that they represent single Ho adatoms and superposition of molecular models suggests non-covalent interaction. At several places (red outlines), novel structural motifs are expressed by the molecules even in the absence of nearby Ho atoms indicative of a minority species having undergone a chemical transformation. It is noteworthy that in our previous investigations,^[26,46] with the same molecule and surface, but without Ho, we have never observed changes below 300 K. However, the irregularity of the arrangements prevents a conclusive analysis of the chemical transformation, where presumably metastable configurations interfere.

To obtain a clearer picture, we annealed the same sample at 200 K. Again, molecules are distributed inhomogeneously contrasting the original periodic assembly. The Ho centers are hardly seen anymore, mainly as larger clusters appearing at step edges. Isolated molecular dimers (Figure 2b) coexist with small clusters and extended aggregates (Figure 2c). Analyzing the dimer motif with enhanced false-color contrast allows recognizing one depression (arrow in Figure 2b) next to a molecular leg. A similar depression was considered a fingerprint for a negatively charged alkynyl moiety resulting from the detachment of H.^[48,50] Accordingly, we superpose molecular models, in which the functional group adjacent to the depression represents an alkynyl moiety and suggest that the dimer motif is stabilized through a hydrogen bond (green line), where the pristine alkyne moiety acts as H donor and the π -system of the alkynyl moiety represents the H acceptor, similar to established T-type bonding schemes in molecular crystals.^[51] Since we observe significant local changes in molecular coverage already for samples without Ho dosage, that is, a growth mode where

some Ag terraces are completely covered by supramolecular assemblies while others are completely free of Ext-TEB, we confidently exclude potential molecular desorption upon Ho dosage at temperatures between 100 and 200 K.

The trimer motifs, where two monomers point toward the central part of a third molecule (see red dashed contour in Figure 2c) can be rationalized in a consistent manner. Herein, the structural arrangements strongly indicate that the most central functional group is again dehydrogenated (see inset of right panel), whence the trimer motif is stabilized by an ionic hydrogen bond^[50,52] with the neighboring phenyl moieties (see red-colored circle segment) and a conventional H bond from an intact alkyne to a nearby π -cloud (green line). A similar trifurcated ionic hydrogen bond arrangement was observed recently for Ext-TEB on Cu(111).^[50] As shown by the superimposed molecular models, the seemingly irregular arrangement of the more extended aggregates can be systematically explained by such binding motifs. Counting their occurrence within several STM images, we infer that around 11 % of terminal alkynes are deprotonated through the interaction with Ho. The proposed reaction Scheme is depicted in Figure 1, left part.

To obtain complementary insights from theory, we performed DFT-based transition-state calculations^[53] investigating tautomerization and dehydrogenation pathways as two possibilities for Ho-initiated reactions. To avoid prohibitively extensive calculation efforts, we employed the smaller derivative 1,3,5-triethynyl-benzene (TEB). The respective initial, transition, and final state images (top and side-views) are depicted for each reaction route, that is, tautomerization (dehydrogenation) in Figure 3a(c). In Figure 3b, the corresponding energy profiles reveal that dehydrogenation expresses a significantly lower activation barrier (1.2 eV) than tautomerization (1.95 eV). In com-

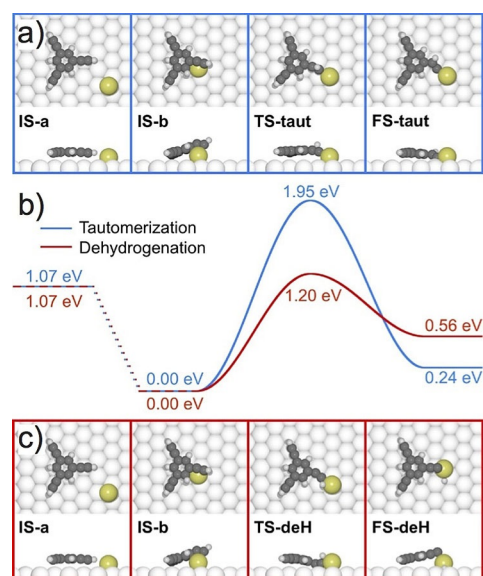


Figure 3. Simulated pathways for Ho-initiated tautomerization and dehydrogenation of terminal alkynes. (a,c) Top and side-views of calculated initial state (left columns IS-a and IS-b), transition state (middle column TS) and final state (right columns FS) are depicted for each path. (b) Energy profiles showing the barriers for Ho-initiated dehydrogenation (red curve) and tautomerization (blue curve).

parison, the direct dehydrogenation without any adatom exhibits a barrier of 1.82 eV as reported earlier.^[53] Thus, theory indicates a pronounced catalytic effect of the related metal-supported Ho atom.

Interestingly, the top-view of the final state image in Figure 3c shows that the cleaved H atom remains bound to the Ho center. Already decades ago, the strong affinity of 4f metal elements toward hydrogen was reported in the case of lanthanide films forming 4f metal dihydride (MH₂) structures.^[54] Individual lanthanide hydride species were identified with high-resolution tunneling microscopy on silver surfaces.^[55,56] First-principle simulations yield that Y³⁺ ions attached to carbon nanotubes are capable to store up to six hydrogen atoms, respectively.^[57] Therefore, we suggest hydrogen uptake at Ho centers, that is, adsorbed Ho-hydride species are generated as side product of the Ho-induced dehydrogenation reaction.

To test the existence of metastable Ho hydride species we prepared samples where Ho and Ext-TEB were deposited at ≈ 110 K, directly followed by transfer to the LT-STM at cryogenic conditions. We observe monodisperse sphere-shaped protrusions scattered between molecular patches irrespective of the sequence of deposition (Ho prior/after Ext-TEB: Figure S3 b,a). The close-up STM image depicted in Figure S3 c allows comparing the isolated Ho species with Ho incorporated in the molecular patches. A significant difference of ≈ 0.2 Å in their apparent height (SI Figure S3 c,d) confirms the different chemical character. Thus, we attribute the green species with Ho-hydride and the yellow with pristine Ho. Related to the latter case, selective interactions between lanthanide atoms and aromatic carbon structures are known.^[58] They are explained by a donation-backdonation mechanism, that is, interactions between the π -orbitals of Ext-TEB and d orbitals of Ho (π -d bonding) according to the Dewar-Chat-Duncanson model.^[57,59] However, the significantly larger distances between the Ho atoms and nearby organic moieties suggest a different interaction mechanism involving mainly weak non-covalent forces. Upon annealing at 200 K the monodisperse protrusions do not persist confirming their metastable character.

Ho-catalyzed dimerization at 130 K

We investigated the potential of Ho towards triggering coupling reactions at low temperatures by preparing a sample where first a sub-ML amount of Ext-TEB was deposited at 130 K and then a small amount of Ho (ca. 0.01 ML) was dosed at 130 K. The sample was immediately transferred to the STM. In Figure 4a, one can identify network-like arrangements containing Ext-TEB monomers and Ho atoms (yellow). Based on the similarity to the previous structural motifs (Figures S2 and S3), we associate them to intact molecules and pristine Ho atoms. More importantly, we also encounter a novel species tentatively interpreted as a covalent dimer (blue rectangle). A close-up image of a similar situation allows identifying the kink in the connection of the two original monomers (Figure 4b, left panel). The size and shape of the species is consistent with a molecular model assuming that a coupling reaction has formed a central vinyl-ethynyl bridge (Figure 4b, right panel)

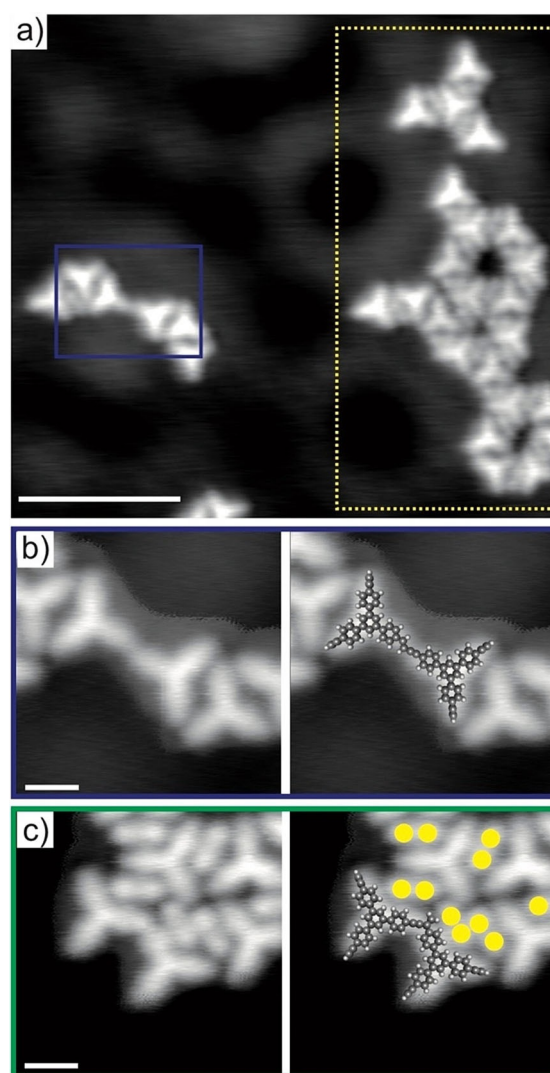


Figure 4. Ho-initiated C–C coupling of Ext-TEB at ca. 130 K. (a) Covalent dimer formed at 130 K (blue frame, see (b)). Yellow framed region (dashed) shows metastable arrangements containing Ho and Ext-TEB monomers (see (c)). (b,c) Covalent enyne regioisomers (dimers) with superimposed molecular models (adjoined images). Metastable bonding motif in (c) comprised of Ho (yellow dots) next to Ext-TEB monomers. Preparation details: Ho dosage (0.01 ML Ho) at 130 K, followed by molecular deposition (4 min) at 130 K, no sample annealing. Tunneling parameters V_t , I_t : (a–c) -0.01 V, 0.1 nA. Scale bars: (a) 6 nm; (b,c) 1 nm.

Further inspection of the sample reveals the existence of a second dimer species depicted in Figure 4c, where a molecular assembly is shown hosting Ho between ethynyl-phenyl moieties of adjacent Ext-TEB. Its shape can be rationalized by assuming a *syn* regioisomer of the enyne bridge.

With the very minute amount of reacted species, it is important to exclude spurious effects, such as reactions at specific sites (impurities, kinks) before Ho-initiated coupling can be concluded. Therefore, we probed the reaction yield by preparing a sample where a higher amount of Ho (0.043 ML) was dosed onto a sub-ML Ext-TEB at 130 K, whereby the sample was kept at that temperature for 30 min after Ho dosage. Under this condition, the before mentioned metastable structures are absent, as can be seen in the overview LT-STM image

in Figure 5a. In contrast, we observe irregular molecular aggregates consisting of a high percentage of dimers and oligomers. The bright protruding features appearing higher than the conjugated backbone of the molecules are attributed to Ho clusters. The close-up image in Figure 5b depicts such a Ho feature, which is indicated by a dashed circle (yellow) surrounded by two monomeric and two dimeric organic species. A detailed look on the dimeric head-to-head coupling motif reveals that the two connected alkynes are slightly offset perpendicular to the connecting axis (blue lines), as discussed before (cf. Figure 5b). Therefore, we attribute the quasi-linear coupling again to a covalent vinyl-ethynyl linkage, that is, an enyne motif.

Besides dimers, also oligomers are encountered, as shown in the top panel of Figure 5c. The shown section of an STM image displays an oligomer expressing a kink connection (green lines and arrow). Its shape is rationalized by the superimposed molecular model (central panel of Figure 5c) com-

posed of five concatenated Ext-TEB monomers. In the bottom panel of Figure 5d, the chemical structure model displays the four enyne motifs. For explaining both, the quasi-linear and the kinked linkages, we propose a Ho-catalyzed coupling of two terminal alkynes to an enyne motif (Figure 5d). Related enyne products resulting from terminal alkyne dimerization were reported by Nishiura et al. using lanthanide half-metallocene complexes as catalytic agents for solution-based reactions.^[60]

Ho-catalyzed cyclotrimerization reaction

To further explore the potential of Ho-assisted coupling reactions, we prepared a sample with Ho dosed at 200 K. After dosing minute Ho amounts of ~0.001–0.007 ML on a sub-ML adlayer of Ext-TEB (molecules and Ho deposited at 200 K) and maintaining a sample temperature of 200 K for 30 min, we again observe the irregular arrangements of monomers, dimers and oligomers (cf. Figure 6a aside organic islands and Figure S4b).

Upon closer inspection (Figure 6b), one can identify both the quasi-linear species and the kink-shaped enyne regioisomer (blue and green outlines) known from previous preparations. Furthermore, two novel species expressing threefold coupling motifs (orange and red) exist. In analogy to previous reports,^[61, 62] we attribute the novel products to regioisomers emanating from cyclotrimerization reactions. The trimeric molecular models above the respective STM images consistently explain the observed products (Figure 6b). For a simplified comprehension that the original monomers are joint by the reaction, the models are color-coded. We differentiate symmetric and asymmetric isomers of the cyclotrimers, rationalized by 1,3,5-trisubstitution (red outline) and 1,2,4-trisubstitution (orange outline) of the central phenylene moiety, respectively. We did not observe additional reaction products besides 1,2,4- and 1,3,5-cyclotrimerization motifs, that is, alkyne cyclotetramerization and butadiyne-forming homocoupling are absent.

Although the high-resolution STM contrast within the 1,2,4-trimer (orange outline in Figure 6b) reveals two nodal planes (arrows) potentially indicating non-covalent bonding between molecular fragments, we confidently exclude Ho-induced monomer fragmentation and uncontrolled side reactions based on the following reasons. First, lateral manipulations on various dimer and trimer species (see Figure S5) evidence their structural integrity upon STM tip-induced lateral displacements on the surface, which indicates the presence of strong bonds between the subunits. Second, the asymmetric trimer motif always expresses the same geometry and STM appearance characterized by the identical locations of nodal planes with respect to the molecular orientation. The comparison with the structural model (top panel of Figure 6b) indicates that the two clear relative depressions (nodal planes) coincide with two phenyl rings (marked by arrows), which experience mutual steric repulsion due to their close vicinity.

We thus rationalize the STM appearance by out-of-plane rotations of the pertaining two phenyl units, thereby relaxing intramolecular stress within the trimer. Non-planar phenyl moieties may locally decrease the STM tunneling conductance due

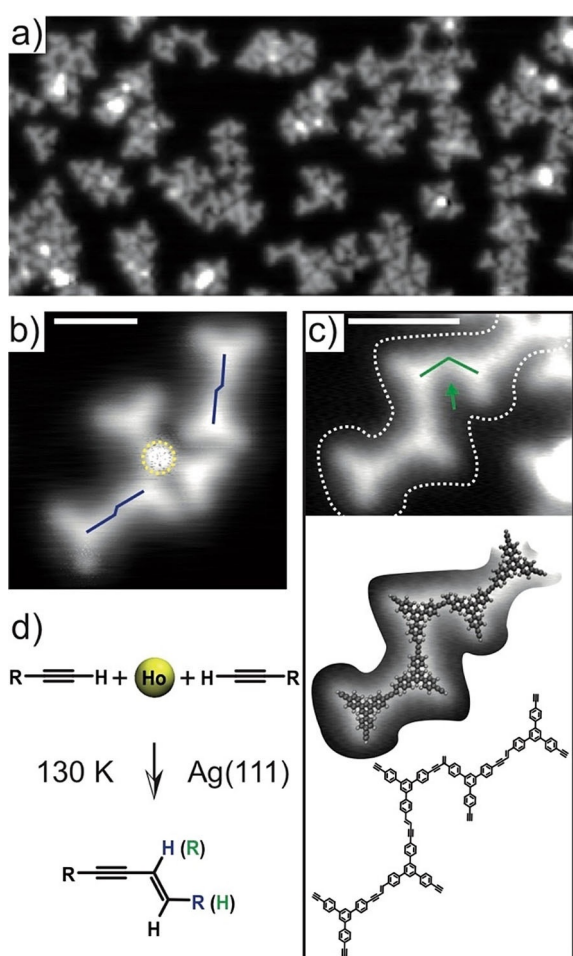


Figure 5. STM results for a preparation with sample held at 130 K after dosing ca. 0.043 ML Ho. (a) Dissolution of islands and formation of covalent structures. (b) Dimers next to a Ho center (dotted yellow circle) express quasi-straight linkage (blue outline). (c) Cut-out of STM image showing a covalent molecular chain with superimposed oligomer model (hydrogen (white) and carbon (grey)). It contains a kink-shaped enyne regioisomer (green arrow). (d) Proposed Ho-assisted reaction path generating twofold coupling via ethynyl-vinyl catenation (two enyne regioisomers marked in blue and green). Tunneling parameters V_t , I_t : (a–c) 0.5 V, 0.1 nA. Scale bars: (a) 10 nm; (b) 2 nm; (c) 3 nm.

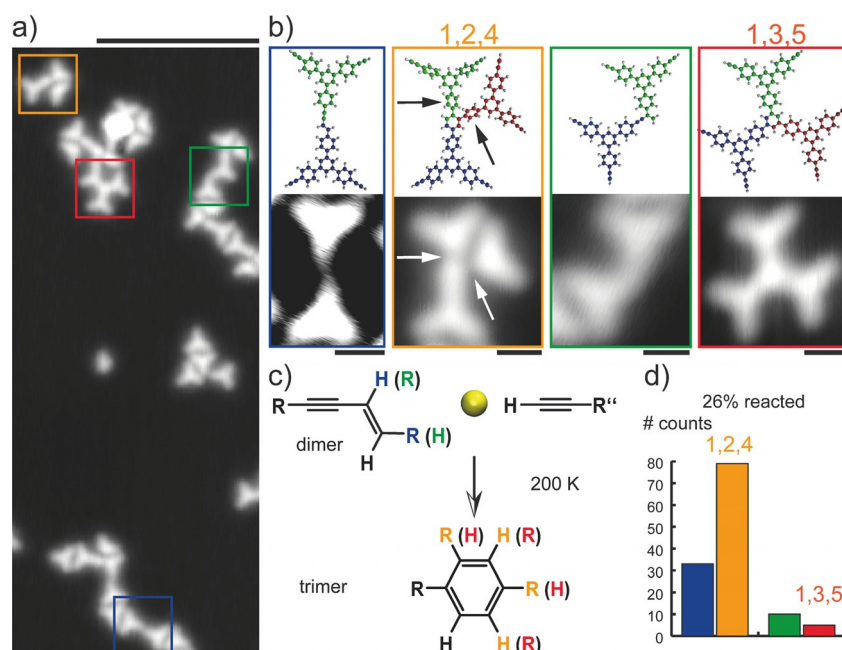


Figure 6. STM results showing cyclotrimerization products formed at 200 K. (a) Coexistence of dimeric and trimeric structures (four species within colored rectangles) (≈ 0.002 ML Ho). (b) High-resolution images of the two regioisomeric dimers (blue and green frames) and two regioisomeric cyclotrimers (orange and red frames). (c) Second step of Ho-induced reaction path generating 1,2,4- (orange) and 1,3,5-cyclotrimers (red). (d) Statistical counting of dimeric and trimeric linkage motifs within a 100×100 nm²-sized region with 127 coupling motifs. Curved arrows indicate possible transitions from intermediates to products. Tunneling parameters V_t , I_t : (a) 0.5 V, 0.1 nA; (b) from left to right: 0.05 V, 0.3 nA; 0.5 V, 0.1 nA; 0.3 V, 0.3 nA; 0.05 V, 0.3 nA. Scale bars: (a) 10 nm; (b) 1 nm.

to a reduction of the orbital overlap with STM tip states, thereby causing reductions of the STM apparent height.

To verify our interpretation from a theoretical standpoint, density functional theory (DFT) calculations including the Ag(111) surface were performed. Figure 7a,c presents top (upper panel) and side-view (lower panel) visualizations of the DFT-modeled Ext-TEB trimers of both asymmetric and symmetric shape, respectively. From the side-view in Figure 7a, one notices the strong tilt of two phenyl rings (marked arrows). According to the top-view (top panel), the tilted phenyls (arrows) are those connected in 1 and 2 position to the central arene ring. The STM image simulation of this structure (Figure 7b) exhibits two relative depressions of the molecular backbone at the respective locations (arrows) in good agreement with the experimental appearance. For comparison, we also present simulations of the symmetric 1,3,5-cyclotrimer (Figure 7c) with nearly planar conformation on Ag(111), reflecting only minor amounts of steric constraints between adjacent phenyl moieties. Accordingly, the associated STM simulation image in Figure 7d reveals a more uniform STM contrast throughout the backbone, where the higher corrugation is absent. Within the trimeric compounds, there is a very good agreement between the simulations (Figure 7b,d) and the experimental STM appearance (orange and red outlines in Figure 6b) of both three-fold coupling motifs. Thus, we exclude molecular fragmentation and non-covalent bonding scenarios as explanation for the orange species.

The absence of trimers for samples prepared at 130 K, and the coexistence of dimers and trimers for sample preparation at 200 K (Figure 6) suggests that the dimeric motif represents

the intermediate for the cyclotrimerization reaction. Accordingly, we propose a Ho-assisted two-step reaction scheme involving two coupling steps (cf. Figure 1, right part). The first step of this reaction is associated with the twofold coupling pathway illustrated in Figure 5d. The second step comprises the Ho-mediated coupling between one dimer unit and one pristine monomer as schematically depicted in Figure 6c. The colors of H and R moieties are consistent with the color-coding above (cf. Figure 5) and describe the two regioisomeric configurations for both the dimeric intermediates and trimeric products, respectively.

Our proposed two-step model agrees with previous reaction studies on ethyne (C_2H_2) cyclotrimerization on Pd(111), where a species of stoichiometric C_4H_4 is reported as an intermediate for benzene production.^[63, 64] However, it was reported that the reaction does not engage C–H bond scission.^[65, 66] Also the acetylene to benzene cyclotrimerization pathway on Cu(110) includes the creation of a related hydrocarbon intermediate (of stoichiometry C_4H_4), with desorption being the rate-limiting process.^[67, 68] In contrast to the computational study on cyclotrimerization on Au(111) of Zhou et al. proposing an intermediate expressing carbon–gold bonds,^[62] to which the enyne intermediate of the present Ho-catalyzed cyclotrimerization on Ag(111) appears to contain only carbon atoms with organic bonding partners (C and H). This indicates the absence of organometallic bonding with catalytic centers (Ho) as well as with surface atoms at the intermediate state. Consistently, the STM simulations of the trimeric products identify them as containing fully hydrated central arene moieties, rendering H abstraction during the enyne formation step unlikely.

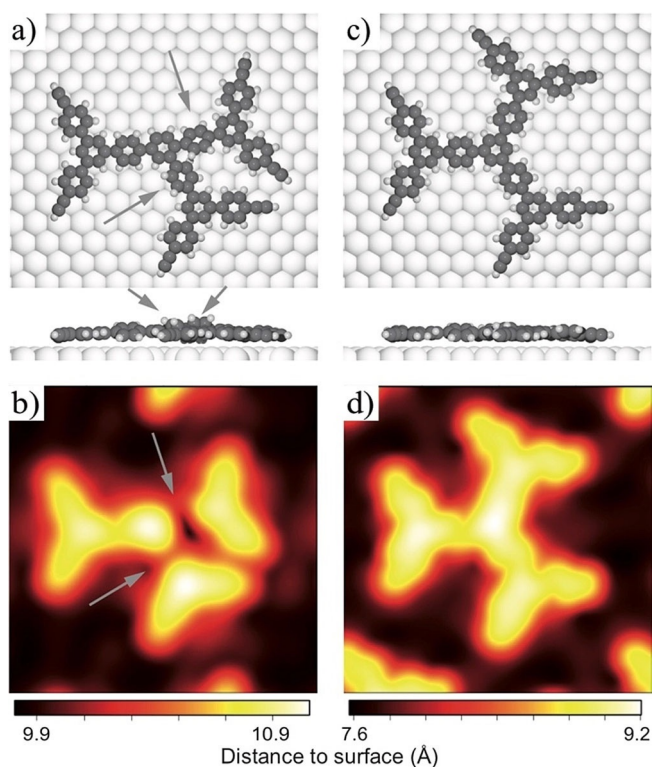


Figure 7. DFT modeling of cyclotrimerization products including the Ag(111) surface. (a,c) Visualizations of (a) 1,2,4- and (c) 1,3,5-cyclotrimer. Upper and lower panel show top and side views, respectively. Marked arrows in (a) indicate rotated phenyl units. (b,d) Simulated STM images for the corresponding structures in (a,c). Marked arrows in (b) indicate nodal planes (cf. Figure 6b). The image in (b) was obtained for constant integration of the local density of states (between E_F and $E_F + 0.5$ eV), corresponding to a constant-current image at $V_t = 0.5$ V. The image in (d) was achieved at a constant value of the local density of states around the Fermi level, corresponding to a constant-current image obtained at small bias. Lateral width of simulation images: 40 Å.

To quantitatively compare the ratios of dimeric and trimeric regioisomers, a 100×100 nm²-sized region featuring 127 coupling motifs was statistically evaluated, results are depicted in the histogram in Figure 6d. The ratio between twofold ethynyl-vinyl linkage and threefold cyclotrimerization products is approximately 1:2. Within enyne compounds (blue and green bars), a ratio of roughly 3:1 indicates that quasi-linear dimers (blue) are strongly favored over the kinked species (green). Within the trimeric compounds (orange and red), a striking ratio of around 16:1 implies the strong dominance of asymmetric coupling over 1,3,5-linkages. Noteworthy, for Ho dosage at 130 K (cf. Figure 5), we observed a similar excess of the quasi-linear species over the kinked dimer suggesting that the dimer to cyclotrimer reaction step hardly changes the ratio between the two intermediate species.

The predominance of asymmetric cyclotrimerization products can be explained under the assumption that during the Ho-mediated reactions C–C bonds are modified without complete rupture. Comparing the coupling motifs, one notices a different number of C atoms connecting adjacent monomer backbones. There are four (three) C atoms for the quasi-linear (kinked) dimer species, while three (two, three and four) C

atoms are found for the symmetric (asymmetric) cyclotrimer. Consequently, the quasi-linear dimers (blue) can react further to form 1,2,4-cyclotrimers but not 1,3,5-compounds, while the kinked intermediates (green) can afford either asymmetric or symmetric forms of cyclotrimerization (see arrows in Figure 6d). This indicates that the very rare 1,3,5 cyclotrimer could only evolve from the already rare kinked intermediate (green outline), while the dominant 1,2,4 trimer emanates from both the frequent and the rare intermediates.

For a further characterization of the coupling reaction we investigated the influence of the annealing time on the reaction yield. We prepared a sample reproducing the previous conditions (first Ext-TEB, then Ho at 200 K), but this time without performing annealing after Ho dosage, i.e., the sample was immediately transferred into the STM and cooled down. Comparing this sample (SI Figure S4e–h) with the previous (Figure S4a–d), it is clear that a qualitatively very similar coupling behavior is observed. We evaluated the number of pristine and reacted alkynes within several 100×100 nm² STM topographs. The relative abundance of the different dimer and trimer species are displayed in the histograms in Figure S4a,e where also the total reaction yields are given. The number of alkynes having reacted to on-surface coupling motifs is independent on the sample annealing time at 200 K, that is, the reaction yield for on-surface coupling (8%) does not increase compared to sample preparations, where the temperature of 200 K is kept for 30 min after Ho dosage. The result indicates that coupling occurs shortly after the arrival of Ho on the surface. Several criteria are relevant to explain such a behavior of the system, that is, where the initially high reactivity strongly decreases with the time after Ho dosage:

- Ho adatoms only trigger reactions when directly hitting reactive groups at their arrival on the surface (Eley–Rideal mechanism).^[69]
- Transiently hot or thermally diffusing single Ho adatoms initiate coupling when hitting molecules which are in thermal equilibrium with the substrate.
- Only monatomic Ho adatoms activate C–C coupling, while clusters or hydrogenated species are catalytically inactive, thus the system expresses dynamic heterogeneity.^[44]

We tried to estimate the involved probability for case (i) by performing random number-based simulations similar to hit-and-stick models, in which we assumed that an arriving Ho atom triggers a reaction when it hits a site occupied by a molecule according to our experimental Ho and Ext-TEB coverages. We estimated the reaction yields as a function of the effective reaction cross-section modeled by the area of reactive sites attributed to a molecule (see Supporting Information). Within this model, Ho atoms are randomly distributed on a 2D array of sites particularly decorated with Ext-TEB molecules. If one Ho atom hits a lattice site occupied by a molecule, we count this event as one reaction step within the scheme of this two-step cyclotrimerization reaction. According to the proposed reaction mechanism in Figure 1, right part, a molecule hit by one (two) Ho atoms counts for C–C coupling toward an

enyne dimer (cyclotrimer). Summing up all reaction steps, the reaction yield for on-surface coupling is obtained. For each STM image, the modeled value was compared with the experimental reaction yields, in order to obtain the respective cross-section. To obtain more statistics, different STM images were evaluated. Since the effective cross-sections are scattered within a large interval ranging from 0.2 to 5.9 nm², the result does not allow a clear distinction of case (i) versus (ii) on the basis of the hit-and-react model.

However, a purely Elay–Rideal mechanism seems unreasonable, since there is a critical substrate temperature below which covalent C–C linkage is absent (i.e., Ho dosage at 105 K instead of 130 K does not lead to intermolecular C–C bond formation). On the other hand, fully thermalized Ho exposures do not trigger coupling reactions. Thus, we conclude that the coupling mechanism relies on catalytically active single Ho atoms, most likely uniting aspects of (ii) and (iii). Hereby the distinction between transiently “hot” or thermally diffusing single Ho adatoms is challenging. It is well known that the adsorption energy dissipation of gas atoms may entail appreciable lateral displacements.^[70] However, for metals the transient diffusion typically comprises only a few lattice constants,^[71] even though the case of lanthanides was not investigated to date.

If this on-surface coupling reaction solely originated from non-thermalized effects during the equilibration of impinging atoms, a metal different from Ho could also trigger C–C coupling in a similar way. To demonstrate the peculiarity of Ho, we dosed the 3d element Pd in a similar way (metal sublimation by heating a Pd wire) on a sub-ML of Ext-TEB on Ag(111). Intriguingly, under these conditions, Pd activates the formation of organometallic Pd-acetylide structures but no covalently coupled species can be identified (Figure S6a–c). Hence, the activity of the arriving Ho atom is significantly different compared to Pd atoms, wherefore we assume that the chemical properties of Ho are crucial for steering low-temperature alkyne coupling on surfaces.

Finally, we showcase the feasibility of Ho-mediated on-surface coupling reactions to synthesize oligomeric carbonaceous nanostructures or 2D networks. Already for low Ho amounts (0.002–0.007 ML) (molecules and Ho deposited at 200 K, maintaining sample at 200 K for 30 min), we observe the occurrence of more extended scaffolds. Figure 8a displays a covalent structure where all linkages are comprised of 1,2,4-cyclotrimerization motifs highlighted in orange. Moreover, imaging its backbone contrast exhibits the two characteristic depressions nearby each coupling node (cf. Figure 8b). Thus, the scaffold can be consistently rationalized by the chemical structure depicted in the bottom panel. For facile identification, the positions of the tilted phenyl rings following from the model are highlighted by dotted purple rectangles. The more regular pattern in Figure 8b shows a hydrocarbon structure mainly containing 1,3,5-trisubstituted benzene moieties as coupling nodes which are highlighted in red in the structure scheme (lower panel). At the top, a linkage section not expressing threefold symmetry can be identified. We tentatively associate it with a twofold linkage motif (blue color) next to an unreacted alkyne moiety. This quasi-linear dimerization intermediate

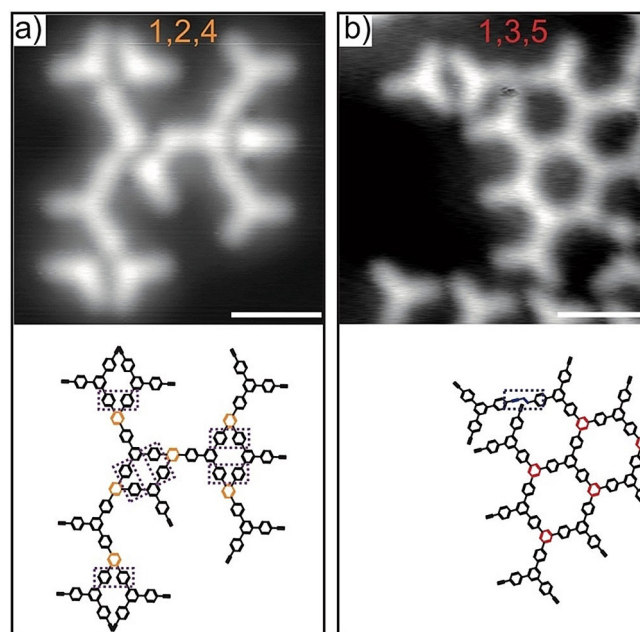


Figure 8. Oligomeric networks expressing threefold coupling nodes formed at 200 K. (a) Covalent scaffold expressing 1,2,4-cyclotrimerization motifs (orange-colored) (same preparation as in Figure 6a). Dotted purple rectangles highlight tilted phenyl moieties producing depressions in the appearance of the molecular backbone. (b) Scaffold mainly expressing 1,3,5-cyclotrimerization nodes (red-colored) featuring honeycomb pores (Ho concentration: ≈ 0.007 ML). One linkage motif (blue rectangle) is recognized as intermediate. Tunneling parameters V_t , I_t : (a) 0.5 V, 0.1 nA; (b) 0.05 V, 0.3 nA. Scale bars: (a,b) 2 nm.

reacts further to form a 1,2,4-trisubstituted arene ring. The corresponding structure models in Figure 8a(b) reveal how molecules involved in 1,2,4- and 1,3,5-cyclotrimerization span rhomboid- and hexagonal-shaped cavities, respectively.

Conclusions

In summary, the potential of Ho-mediated low-temperature reactions has been recognized for interfacial chemical conversions on a noble metal support. The catalytic activity of thermalized Ho initiates deprotonation of terminal alkyne units below 200 K down to ≈ 100 K. In addition, Ho adatoms dosed on a sub-ML of intact molecules initiate intermolecular covalent linkages. Importantly, enyne-forming dimerization occurs already at $T \approx 130$ K, while cyclotrimerization requires only slightly higher substrate temperatures of $T \approx 200$ K. Both 1,3,5- and 1,2,4-trisubstitution motifs coexist within naturally occurring trimers and extended oligomers.

Our findings lend support to associate mobile isolated adatoms with active sites in heterogeneous catalysis, thus substantiating conceptual view expressed in other contexts.^[45,71] It will be valuable to consider these effects in future computational catalyst screening efforts.^[72] Notably, the reactions proceed in a temperature regime where preassembled structures held together by weak interactions, such as H-bonding, should be stable. This opens novel avenues for on-surface synthesis contrasting, for instance, the popular Ullmann coupling/cyclodehy-

drogenation approach,^[73,74] where significantly higher annealing temperatures (500–600 K) are required.

Since the reaction proceeds in the presence of minute amounts of catalytic Ho on an otherwise inert surface, it is supposed to be operational also on top of different substrates with limited reactivity, including possibly even dielectric surface layers or 2D sheet materials. The regioselectivity between 1,3,5- and 1,2,4-cyclotrimerization nodes may be further optimized on 2D sheet materials by using a different lanthanide element or by employing tailored organolanthanide complexes as catalytic agent.^[60] In addition, metal-organic coordination networks with coordinatively unsaturated lanthanide centers might be useful templates for organizing the catalytic centers, thereby enabling improved control on the structural properties of on-surface formed covalent nanostructures and reticulations.

Methods

Details on experiments

Sample preparation and STM characterization were conducted with a commercial Joule–Thompson scanning tunneling microscope system (www.specs.de) with an ultra-high vacuum base pressure below 1×10^{-10} mbar. The surface of a Ag(111) crystal was smoothed and cleaned by several cycles of Ar⁺ sputtering (0.9 kV, 10 μ A sputter current, 25 min) and subsequent annealing at 750 K for 15 min. Details on the synthesis of the molecule can be found in ref.^[26] After careful degassing, the molecule was deposited from an evaporation cell kept at 400–420 K on the clean surface kept at 200 or 250 K to avoid homocoupling of terminal alkynes. Afterward, Ho atoms were deposited on the sample kept at constant temperature (at 100–130 K or at 200 K) by cooling the manipulator with liquid nitrogen and simultaneously counter-heating the sample. Sample temperatures were directly measured at the Ag(111) crystal (sidewise) via a Type K thermocouple wire (Chromel/Alumel). A beam of Ho atoms was created through resistive heating of a thin Ho foil (Mateck) with a purity of 99.9%. Pd metal atoms were dosed from a high-purity Pd wire wound around a tungsten U-bolt guiding a heating current. An etched tungsten tip was used to obtain STM images in the constant-current mode at 4.4 K.

Details on simulations

For creating structure models of monomers and oligomers we used the Chemdraw software.^[75] Gas-phase structure relaxation was performed via the Hyperchem software^[76] using the semi-empirical method AM1. The model visualizations were achieved by employing the VMD software.^[77]

Periodic DFT calculations were performed with the VASP code,^[78] using the projector-augmented wave method^[79] and plane waves expanded to a kinetic energy cutoff of 400 eV. Exchange-correlation effects were described by the van der Waals density functional (vdWDF)^[80] using rev-vdWDF2^[81] for trimers and optB86b-vdWDF^[82] for reaction pathways. Two dif-

ferent functionals were used to ensure that pathways were calculated with the exact same settings as previous pathway calculations for the TEB molecule on Ag(111),^[53] although the two functionals have shown to describe adsorption of molecules with equal precision.^[83] The Ag(111) surface was represented by a four layered slab, and a p(13 \times 12) unit cell for the 1,3,5-cyclotrimer, a rectangular 13 \times 12 unit cell for the 1,2,4-cyclotrimer, and a p(7 \times 7) unit cell for the reaction pathway calculations, together with a Γ -point only k-point sampling in all cases. Reaction pathways were calculated with the Climbing Image Nudge Elastic Band (CI-NEB)^[84] and Dimer^[85] methods. All structures were structurally optimized until the forces on all atoms, except the two bottom layers of the Au slabs, were smaller than 0.01 eV \AA^{-1} . STM images were simulated with the Tersoff–Hamann approximation^[86] with the implementation by Lorente and Persson.^[87]

Acknowledgements

Funding provided by the ERC Advanced Grant MolArt (grant no. 247299), the TUM Institute of Advanced Studies, and the German Research Foundation via KL 2294/6-1 is gratefully acknowledged.

Conflict of interest

The authors declare no conflict of interest.

Keywords: carbon coupling · cyclotrimerization · lanthanides · on-surface synthesis · terminal alkynes

- [1] A. Wittstock, V. Zielasek, J. Biener, C. M. Friend, M. Baumer, *Science* **2010**, *327*, 319–322.
- [2] T. Ishida, M. Haruta, *Angew. Chem. Int. Ed.* **2007**, *46*, 7154–7156; *Angew. Chem.* **2007**, *119*, 7288–7290.
- [3] K. C. Gupta, A. K. Sutar, *Coord. Chem. Rev.* **2008**, *252*, 1420–1450.
- [4] D. Astruc, F. Lu, J. R. Aranzas, *Angew. Chem. Int. Ed.* **2005**, *44*, 7852–7872; *Angew. Chem.* **2005**, *117*, 8062–8083.
- [5] L. Li, W. W. Brennessel, W. D. Jones, *J. Am. Chem. Soc.* **2008**, *130*, 12414–12419.
- [6] B. D. Sherry, A. Furstner, *Acc. Chem. Res.* **2008**, *41*, 1500–1511.
- [7] P. Kissel, R. Erni, W. B. Schweizer, M. D. Rossell, B. T. King, T. Bauer, S. Götzinger, A. D. Schlüter, J. Sakamoto, *Nat. Chem.* **2012**, *4*, 287–291.
- [8] W. Liu, X. Luo, Y. Bao, Y. P. Liu, G.-H. Ning, I. Abdelwahab, L. Li, C. T. Nai, Z. G. Hu, D. Zhao, B. Liu, S. Y. Quek, K. P. Loh, *Nat. Chem.* **2017**, *9*, 563–570.
- [9] R. J. Shannon, M. A. Blitz, A. Goddard, D. E. Heard, *Nat. Chem.* **2013**, *5*, 745–749.
- [10] L. Grill, M. Dyer, L. Lafferentz, M. Persson, M. V. Peters, S. Hecht, *Nat. Nanotechnol.* **2007**, *2*, 687–691.
- [11] G. Otero, G. Biddau, C. Sanchez-Sanchez, R. Caillard, M. F. Lopez, C. Rogero, F. J. Palomares, N. Cabello, M. A. Basanta, J. Ortega, J. Mendez, A. M. Echavarren, R. Perez, B. Gomez-Lor, J. A. Martin-Gago, *Nature* **2008**, *454*, 865–868.
- [12] J. M. Cai, P. Ruffieux, R. Jaafar, M. Bieri, T. Braun, S. Blankenburg, M. Muoth, A. P. Seitsonen, M. Saleh, X. Feng, K. Müllen, R. Fasel, *Nature* **2010**, *466*, 470–473.
- [13] M. Lackinger, *Polym. Int.* **2015**, *64*, 1073–1078.
- [14] F. Klappenberger, Y.-Q. Zhang, J. Björk, S. Klyatskaya, M. Ruben, J. V. Barth, *Acc. Chem. Res.* **2015**, *48*, 2140–2150.
- [15] L. Dong, P. N. Liu, N. Lin, *Acc. Chem. Res.* **2015**, *48*, 2765–2774.

- [16] Q. T. Fan, J. M. Gottfried, J. F. Zhu, *Acc. Chem. Res.* **2015**, *48*, 2484–2494.
- [17] M. Bieri, S. Blankenburg, M. Kivala, C. A. Pignedoli, P. Ruffieux, K. Müllen, R. Fasel, *Chem. Commun.* **2011**, *47*, 10239–10241.
- [18] L. Lafferentz, V. Eberhardt, C. Dri, C. Africh, G. Comelli, F. Esch, S. Hecht, L. Grill, *Nat. Chem.* **2012**, *4*, 215–220.
- [19] N. A. A. Zwaneveld, R. Pawlak, M. Abel, D. Catalin, D. Gimes, D. Bertin, L. Porte, *J. Am. Chem. Soc.* **2008**, *130*, 6678–6679.
- [20] S. Weigelt, C. Busse, C. Bombis, M. Knudsen, K. Gothelf, E. Lægsgaard, F. Besenbacher, T. Linderoth, *Angew. Chem. Int. Ed.* **2008**, *47*, 4406–4410; *Angew. Chem.* **2008**, *120*, 4478–4482.
- [21] A. C. Marele, R. Mas-Balleste, L. Terracciano, J. Rodriguez-Fernandez, I. Berlanga, S. S. Alexandre, R. Otero, J. M. Gallego, F. Zamora, J. M. Gomez-Rodriguez, *Chem. Commun.* **2012**, *48*, 6779–6781.
- [22] J. F. Dienstmaier, D. D. Medina, M. Dogru, P. Knochel, T. Bein, W. M. Heckl, M. Lackinger, *ACS Nano* **2012**, *6*, 7234–7242.
- [23] L. Jiang, A. C. Papageorgiou, S. C. Oh, O. Saglam, J. Reichert, D. A. Duncan, Y.-Q. Zhang, F. Klappenberger, Y. Guo, F. Allegretti, S. More, R. Bhosale, A. Mateo-Alonso, J. V. Barth, *ACS Nano* **2016**, *10*, 1033–1041.
- [24] M. Abel, S. Clair, O. Ourdjini, M. Mossayan, L. Porte, *J. Am. Chem. Soc.* **2011**, *133*, 1203–1205.
- [25] B. Yang, J. Björk, H. Lin, X. Zhang, H. Zhang, Y. Li, J. Fan, Q. Li, L. Chi, *J. Am. Chem. Soc.* **2015**, *137*, 4904–4907.
- [26] Y.-Q. Zhang, N. Kepcija, M. Kleinschrodt, K. Diller, S. Fischer, A. C. Papageorgiou, F. Allegretti, J. Björk, S. Klyatskaya, F. Klappenberger, *Nat. Commun.* **2012**, *3*, 1286–1293.
- [27] H.-Y. Gao, H. Wagner, D. Zhong, J.-H. Franke, A. Studer, H. Fuchs, *Angew. Chem. Int. Ed.* **2013**, *52*, 4024–4028; *Angew. Chem.* **2013**, *125*, 4116–4120.
- [28] H.-Y. Gao, J.-H. Franke, H. Wagner, D. Zhong, P.-A. Held, A. Studer, H. Fuchs, *J. Phys. Chem. C* **2013**, *117*, 18595–18602.
- [29] P. A. Held, H. Fuchs, A. Studer, *Chem. Eur. J.* **2017**, *23*, 5874–5892.
- [30] D. F. Perepichka, F. Rosei, *Science* **2009**, *323*, 216–217.
- [31] S. Wan, J. Guo, J. Kim, H. Ihee, D. Jiang, *Angew. Chem. Int. Ed.* **2008**, *47*, 8826–8830; *Angew. Chem.* **2008**, *120*, 8958–8962.
- [32] F. Klappenberger, R. Hellwig, P. Du, T. Paintner, M. Uphoff, L. Zhang, T. Lin, B. A. Moghanaki, M. Paszkiewicz, I. Vobornik, J. Fujii, O. Fuhr, Y. Q. Zhang, F. Allegretti, M. Ruben, J. V. Barth, *Small* **2018**, *14*, 1704321.
- [33] Ref. [10].
- [34] A. P. Côté, A. I. Benin, N. W. Ockwig, M. O’Keeffe, A. J. Matzger, O. M. Yaghi, *Science* **2005**, *310*, 1166–1170.
- [35] S. L. Candelaria, Y. Shao, W. Zhou, X. Li, J. Xiao, J.-G. Zhang, Y. Wang, J. Liu, J. Li, G. Cao, *Nano Energy* **2012**, *1*, 195–220.
- [36] J. Z. Liu, J. W. Y. Lam, B. Z. Tang, *Chem. Rev.* **2009**, *109*, 5799–5867.
- [37] D. Ćija, W. Auwärter, S. Vijayaraghavan, K. Seufert, F. Bischoff, K. Tashiro, J. V. Barth, *Angew. Chem. Int. Ed.* **2011**, *50*, 3872–3877; *Angew. Chem.* **2011**, *123*, 3958–3963.
- [38] J. I. Urgel, B. Cirera, Y. Wang, W. Auwärter, R. Otero, J. M. Gallego, M. Alcamí, S. Klyatskaya, M. Ruben, F. Martin, R. Miranda, D. Ćija, J. V. Barth, *Small* **2015**, *11*, 6358–6364.
- [39] J. Feng, H. Zhang, *Chem. Soc. Rev.* **2013**, *42*, 387–410.
- [40] F. Donati, S. Rusponi, S. Stepanow, C. Waeckerlin, A. Singha, L. Persichetti, R. Baltic, K. Diller, F. Patthey, E. Fernandes, J. Dreiser, Z. Sljivancanin, K. Kummer, C. Nistor, P. Gambardella, H. Brune, *Science* **2016**, *352*, 318–321.
- [41] K. Kim, T. Lee, Y. Kwon, Y. Seo, J. Song, J. K. Park, H. Lee, J. Y. Park, H. Ihee, S. J. Cho, R. Ryoo, *Nature* **2016**, *535*, 131–135.
- [42] J. Adisoejoso, T. Lin, X. S. Shang, K. J. Shi, A. Gupta, P. N. Liu, N. Lin, *Chem. Eur. J.* **2014**, *20*, 4111–4116.
- [43] W. Zhao, L. Dong, C. Huang, Z. M. Win, N. Lin, *Chem. Commun.* **2016**, *52*, 13225–13228.
- [44] N. Lin, D. Payer, A. Dmitriev, T. Strunskus, C. Wöll, J. V. Barth, K. Kern, *Angew. Chem. Int. Ed.* **2005**, *44*, 1488–1491; *Angew. Chem.* **2005**, *117*, 1512–1515.
- [45] J. Y. Liu, *ACS Catal.* **2017**, *7*, 34–59.
- [46] N. Kepcija, Y.-Q. Zhang, M. Kleinschrodt, J. Björk, S. Klyatskaya, F. Klappenberger, M. Ruben, J. V. Barth, *J. Phys. Chem. C* **2013**, *117*, 3987–3995.
- [47] J. Liu, Q. Chen, L. Xiao, J. Shang, X. Zhou, Z. Zhang, Y. Wang, X. Shao, J. Li, W. Chen, G. Q. Xu, H. Tang, D. Zhao, K. Wu, *ACS Nano* **2015**, *9*, 6305–6314.
- [48] Y.-Q. Zhang, M. Paszkiewicz, P. Du, L. Zhang, T. Lin, Z. Chen, S. Klyatskaya, M. Ruben, A. P. Seitsonen, J. V. Barth, F. Klappenberger, *Nat. Chem.* **2018**, *10*, 296–304.
- [49] F. Silly, M. Pivetta, M. Ternes, F. Patthey, J. P. Pelz, W.-D. Schneider, *Phys. Rev. Lett.* **2004**, *92*, 016101.
- [50] Y.-Q. Zhang, J. Bjoerk, P. Weber, R. Hellwig, K. Diller, A. C. Papageorgiou, S. C. Oh, S. Fischer, F. Allegretti, S. Klyatskaya, M. Ruben, J. V. Barth, F. Klappenberger, *J. Phys. Chem. C* **2015**, *119*, 9669–9679.
- [51] T. Steiner, E. B. Starikov, A. M. Amado, J. J. C. Teixeira-Dias, *J. Chem. Soc. Perkin Trans. 2* **1995**, 1321–1326.
- [52] D. Payer, A. Comisso, A. Dmitriev, T. Strunskus, N. Lin, C. Wöll, A. DeVita, J. Barth, K. Kern, *Chem. Eur. J.* **2007**, *13*, 3900–3906.
- [53] J. Björk, Y.-Q. Zhang, F. Klappenberger, J. V. Barth, S. Stafström, *J. Phys. Chem. C* **2014**, *118*, 3181–3187.
- [54] D. D. Eley, D. Needham, *Proc. R. Soc. London Ser. A* **1984**, *393*, 257–276.
- [55] M. Pivetta, M. Ternes, F. Patthey, W. D. Schneider, *Phys. Rev. Lett.* **2007**, *99*, 126104.
- [56] M. Ternes, A. J. Heinrich, W. D. Schneider, *J. Phys. Condens. Matter* **2009**, *21*, 053001.
- [57] B. Chakraborty, P. Modak, S. Banerjee, *J. Phys. Chem. C* **2012**, *116*, 22502–22508.
- [58] R. Baltic, M. Pivetta, F. Donati, C. Wäckerlin, A. Singha, J. Dreiser, S. Rusponi, H. Brune, *Nano Lett.* **2016**, *16*, 7610–7615.
- [59] *Encyclopedia of Inorganic and Bioinorganic Chemistry*, Wiley, Hoboken, **2011**.
- [60] M. Nishiura, Z. Hou, Y. Wakatsuki, T. Yamaki, T. Miyamoto, *J. Am. Chem. Soc.* **2003**, *125*, 1184–1185.
- [61] J. Liu, P. Ruffieux, X. Feng, K. Müllen, R. Fasel, *Chem. Commun.* **2014**, *50*, 11200–11203.
- [62] H. Zhou, J. Liu, S. Du, L. Zhang, G. Li, Y. Zhang, B. Z. Tang, H.-J. Gao, *J. Am. Chem. Soc.* **2014**, *136*, 5567–5570.
- [63] W. Tysoe, G. Nyberg, R. Lambert, *Surf. Sci.* **1983**, *135*, 128–146.
- [64] C. H. Patterson, R. M. Lambert, *J. Am. Chem. Soc.* **1988**, *110*, 6871–6877.
- [65] C. H. Patterson, R. M. Lambert, *J. Phys. Chem.* **1988**, *92*, 1266–1270.
- [66] T. V. W. Janssens, S. Völkering, T. Zambelli, J. Wintterlin, *J. Phys. Chem. B* **1998**, *102*, 6521–6528.
- [67] J. R. Lomas, C. J. Baddeley, M. S. Tikhov, R. M. Lambert, *Langmuir* **1995**, *11*, 3048–3053.
- [68] H. Öberg, Y. Nestsarenka, A. Matsuda, J. Gladh, T. Hansson, L. G. M. Pettersson, H. Öström, *J. Phys. Chem. C* **2012**, *116*, 9550–9560.
- [69] M. Xi, B. E. Bent, *J. Vac. Sci. Technol. B* **1992**, *10*, 2440–2446.
- [70] J. V. Barth, *Surf. Sci. Rep.* **2000**, *40*, 75–149.
- [71] N. N. Negulyaev, V. S. Stepanyuk, L. Niebergall, P. Bruno, W. Auwärter, Y. Pennec, G. Jahnz, J. V. Barth, *Phys. Rev. B* **2009**, *79*, 195411.
- [72] K. Reuter, C. P. Plaisance, H. Oberhofer, M. Andersen, *J. Chem. Phys.* **2017**, *146*, 040901.
- [73] J. A. Lipton-Duffin, O. Ivasenko, D. F. Perepichka, F. Rosei, *Small* **2009**, *5*, 592–597.
- [74] Ref. [12].
- [75] ChemDraw Professional 15.0.
- [76] HyperChem Release 7.0 (Molecular Modeling).
- [77] W. Humphrey, A. Dalke, K. Schulten, *J. Mol. Graphics* **1996**, *14*, 33–38.
- [78] G. Kresse, J. Furthmüller, *Phys. Rev. B* **1996**, *54*, 11169–11186.
- [79] P. E. Blöchl, *Phys. Rev. B* **1994**, *50*, 17953–17979.
- [80] M. Dion, H. Rydberg, E. Schröder, D. C. Langreth, B. I. Lundqvist, *Phys. Rev. Lett.* **2004**, *92*, 246401.
- [81] I. Hamada, *Phys. Rev. B* **2014**, *89*, 121103.
- [82] J. Klimeš, D. R. Bowler, A. Michaelides, *Phys. Rev. B* **2011**, *83*, 195131.
- [83] J. Björk, S. Stafström, *ChemPhysChem* **2014**, *15*, 2851–2858.
- [84] G. Henkelman, B. P. Uberuaga, H. Jónsson, *J. Chem. Phys.* **2000**, *113*, 9901–9904.
- [85] J. Kästner, P. Sherwood, *J. Chem. Phys.* **2008**, *128*, 014106.
- [86] J. Tersoff, D. R. Hamann, *Phys. Rev. Lett.* **1983**, *50*, 1998–2001.
- [87] N. Lorente, M. Persson, *Faraday Discuss.* **2000**, *117*, 277–290.

Manuscript received: June 18, 2018

Accepted manuscript online: July 24, 2018

Version of record online: October 4, 2018